Research Article

Ghalia A. Gaber*, Mohamed Mohamady Ghobashy, Mohamed Madani, Dalal Mohamed Alshangiti, Sheikha A. Alkhursani, Samera Ali Al-Gahtany, and Norhan Nady

Study of the corrosion-inhibiting activity of the green materials of the *Posidonia oceanica* leaves' ethanolic extract based on PVP in corrosive media (1 M of HCl)

https://doi.org/10.1515/gps-2021-0055
received April 09, 2021; accepted July 28, 2021

Abstract: Since the corrosion protection of mild steel samples in corrosive media (1 M of hydrochloric acid [HCl]) was cheap and successful, the ethanol extract of *Posidonia oceanica* leaves based on polyvinylpyrrolidone (*P. oceanica*/PVP) was analyzed using the weight reduction, the open circuit potential, and the potentiodynamic polarization methods. The obtained results explained that the productivity of hindrance increments had the greatest restraint efficiency of ~81% at 1,000 ppm, as the concentration of the extract increased. Liable for adsorption as a thin layer on the surface of mild steel to protect it, the creation of kaolin-traced phenolic and polysaccharide compounds was confirmed by the Fourier transform infrared spectroscopy analysis. A scanning electron microscope was used to evaluate the inhibitive action of *P. oceanica*/PVP against steel in corrosive media and the change in surface morphology was considered. It is presumed that the ethanol removed from the *Posidonia oceanica* leaves can fill in as a compelling consumption inhibitor for gentle steel in HCL solution (1 M).

*** Corresponding author: Ghalia A. Gaber,** Department of Chemistry, Faculty of Science (Girls), Al-Azhar University, P.O. Box 11754, Yousef Abbas Str., Nasr City, Cairo, Egypt,
e-mail: ghaliaasaid@azhar.edu.eg
Mohamed Mohamady Ghobashy: Radiation Research of Polymer Chemistry Department, National Center for Radiation Research and Technology, Egyptian Atomic Energy Authority, P.O. 8029, Cairo, Egypt
Mohamed Madani, Dalal Mohamed Alshangiti, Sheikha A. Alkhursani: Faculty of Science and Humanities, Jubail, Imam Abdulrahman Bin Faisal University, Jubail, Saudi Arabia
Samera Ali Al-Gahtany: Faculty of Science, University of Jeddah, Jeddah, Saudi Arabia
Norhan Nady: Polymeric Materials Research Department, City of Scientific Research and Technological Applications (SRTA-City), Alexandria, Egypt

Keywords: polyvinylpyrrolidone, corrosion, *Posidonia oceanica*, ethanolic extract

1 Introduction

Posidonia oceanica is an indigenous aquatic plant that forms vast meadows, prevents erosion, and hosts several marine creatures in the Mediterranean Sea. Extracts of *P. oceanica* containing antioxidant capacity have been mentioned [1]. Different studies have shown that natural plant-based parts containing different natural mixes have an inhibitive corrosion effect [2]. Plant extracts and natural species, inferred as an ecologically maintainable, sustainable, promptly accessible, and appropriate source of corrosion inhibitors, are essential for their application [3–6]. Amino acids, alkaloids, tannins, and pigments are portions of the constituents of plant products [7]. The amazing green coerosion inhibiting has been utilized. A new generation of corrosion inhibitive pigment based on zinc acetate-*Cichorium intybus* L. leaf extract (ZnA-CIL.L) has been synthesized. Results showed promising corrosion inhibition performance of the hybrid ZnA-CIL.L complex on the steel surface in saline solution [8,9]. Polyvinylpyrrolidone (PVP) is an ecofriendly hydrophilic polymer that is used in this work due to its features, such as its low cost, highly hydrophilic character, and amorphous form [10]. PVP is synthesized by radiation techniques [11–13]. It is a soluble polymer that can form free-standing, thin films (thickness from 50 to 200 μm) using the solution casting method and is easy to remove from the substrate [14]. The absence of PVP causes aggregates or irregular dispersion of *P. oceanica*. Wang and Wang proved that absence of PVP caused the aggregates of Pd nanosheets and PVP did not make any obvious difference in the morphology of nanosheets [15]. In this contact,

PVP has a good, free-standing, thin film forming capability. Additionally, it is a candidate to be used as a film formation in corrosion inhibitor applications because it is cheap and eco-friendly, and is made as a transparent, thin film by a simple casting method.

The current work tests the inhibitive activity of the *Posidonia oceanica* leaves' ethanolic extract based on PVP as a green erosion inhibitor in control of the steel consumption movement in corrosive media (1 M of HCl) using gravimetric techniques and electrochemical strategies.

2 Experimental methods

2.1 Materials

An ethanol-soluble polymer, PVP with an average molecular weight (M_w) of 100 kDa (highly viscous), was purchased from Sigma-Aldrich Chemicals Co. *Posidonia oceanica* leaves were collected from the Mediterranean Sea in Alexandria city.

2.2 Preparation of the ethanolic extracts of *Posidonia oceanica* leaves based on PVP using the solid dispersion technique

Posidonia oceanica leaves were collected from Alexandria in Egypt in July 2019. They were rinsed three times with water (H_2O) to remove gravel and sand before being dried in the drier oven at a temperature of 50°C. Then, they were put in a dry blender to give a fine powder of *Posidonia oceanica* leaves. Finally, the dried powder, along with 30–70% ethanol and isopropanol, refluxed at 75°C for 7 h was recovered three times. Next the appropriate weight of the *Posidonia oceanica* leaves' ethanolic extracts and the PVP powder were dissolved in isopropanol in a ratio of 1:1 wt% to ensure that the ethanolic extracts of *Posidonia oceanica* leaves are well linked to the PVP matrix. The clear solution of the ethanolic extracts of *Posidonia oceanica* leaves and PVP was dried under vacuum. The obtained *Posidonia oceanica* extracts and the PVP powder were ready for corrosion experiments.

2.3 Corrosion experimental setup

The following chemicals were used to make the working electrode of mild steel rod: 0.316 wt% of C; 0.218 wt% of Si, 0.825 wt% of Mn, 0.0869 wt% of Cr, and balance Fe. The rod was inserted into a glass tube and secured with araldite, leaving a 1 cm^2 circular geometric shape to be in touch with the testing solution. For weight-loss measurements, the rod was cut into several coupons; each one has a surface area of 0.785 cm^2. The working anode was cleaned with coarseness emery paper preceding each trial and washed with $(CH_3)_2CO$. Lastly, it was washed with two-fold double-distilled H_2O. While saturated calomel electrode SCE (Hg/Hg_2Cl_2-Sat. KCl) was attached as a reference electrode of normal 25 mL electrolytic cell size, the auxiliary electrode was a platinum layer. By analytically diluting 37% of HCl with double-distilled H_2O, the corrosive media was prepared. This compound ranged in concentration from 100 to 1,000 ppm. To decide the corrosion behavior of the mild steel, chemical and various electrochemical techniques, such as weight reduction estimations, potentiodynamic polarization (PP), and open circuit potential (OCP), were utilized.

2.4 Gravimetric method (weight loss)

Weight reduction estimations were done in a beaker by adding 25 mL of acidic solution (1 M of HCl) with and without (free of) the various concentrations of *P. oceanica*/PVP. The coupons were removed after immersion, then rinsed with double-distilled water and $(CH_3)_2CO$. The experiment was repeated twice and the mean weight-loss value was recorded. The average rate of steel corrosion is calculated using Eqs. 1 and 2 as follows [16]:

$$\Delta W = W_1 - W_2 \tag{1}$$

$$\text{C.R. (mm/year)} = \frac{\Delta W \times K}{A \times T \times D} \tag{2}$$

where K is a constant (8.76×10^4), T is time (h), A is section area (cm^2), ΔW is loss of sample weight (g), and D is density (7.9 g/cm^3). The surface coverage degree (θ) was calculated using Eq. 3:

$$\theta = \frac{W_0 - W_i}{W_0} \tag{3}$$

where W_i and W_0 are estimates of mild steel coupon weight loss in constrained and uninhibited solutions, respectively. The efficiency of inhibition (IE%) was calculated according to Eq. 4:

$$\text{IE\%} = \theta \times 100 \tag{4}$$

2.5 OCP estimations

By studying the alteration in corrosion potential (E_{corr}) over time, the electrochemical characteristic of steel samples in corrosive media was intensified. In the steady-state condition of corrosion excrement, the OCP and the electrochemical calculations were performed. The variation in mild steel corrosion ability in 1 M of HCl was calculated versus SCE in the absence and existence of the diverse inhibitor concentrations of *P. oceanica*/PVP. Over a 30 min exposure interval, the time dependence of OCP was recorded for different experiment conditions. The same sample was used for PP experiments.

2.6 PP estimations

PP curves of steel sample in corrosive media were swept at the rate of 0.5 mV/s between −0.8 and +0.8 V. Prior to the corrosion experiment, the operating electrode was submerged in the test solution for 30 min to provide a quasi-stationary estimate of the OCP. Faraday's law can be used to calculate the rate of corrosion (CR) (weight of steel consumption per year) using Eq. 5 [17]:

$$\text{CR (μm/year)} = 3.3I_{corr}M/zd \tag{5}$$

where z is an ionic charge that equals 3 for iron (Fe), M is the atomic weight (at wt) of metal that equals 55.85 for Fe, d is the iron (Fe) density that equals 7.9 g/cm^3, and I_{corr} is the current density of corrosion which is expressed as μA/cm^2.

The values of corrosion current and potential (I_{corr} and E_{corr}) were measured using the intersection of the linear cathodic and anodic branches of Tafel plots in the presence and absence of various amounts of *Posidonia oceanica* ethanolic extracts. Each experiment was carried out at least three times. Stern–Geary equation was used to resolve the polarization resistance (R_p) values. Eq. 6 [18] is:

$$R_p = \frac{\beta_a \cdot \beta_c}{2.303I_{corr}(\beta_a + \beta_c)} \tag{6}$$

The surface inclusion degrees (θ) were calculated using potentiodynamic measurements by Eq. 7:

$$\theta = 1 - I_{corr}/I_{corr}° \tag{7}$$

where $I_{corr}°$ and I_{corr} are the densities of corrosion current in the absence and existence of *P. oceanica*/PVP, respectively. The inhibitive efficiency (IE%) was measured by Eq. 8:

$$\text{IE\%} = \theta \times 100 \tag{8}$$

2.7 Surface characterization

Scanning electron microscopy (SEM) and energy dispersive X-ray analysis (EDS) were used to examine the surface morphology of corrosive sample products on mild steel after 120 h of immersion in corrosive media of 1 M of HCl in the existence and absence of several concentrations of *P. oceanica*/PVP extracts.

2.8 Fourier transforms infrared (FTIR) spectroscopy

Fourier transform infrared spectrometer (FTIR) (Thermo Scientific-NICOLET iS10 USA) was used to acquire absorption spectra in the infrared band. This method is used to identify the primary functional groups of *Posidonia oceanica*/PVP. Samples were combined with KBr, crushed, and pressed with a specific press to produce a disc with a standard diameter.

2.9 Electrochemical impedance spectroscopy (EIS)

EIS measurements of mild steel were carried out in frequency range from 100 kHz to 100 mHz with amplitude of 10 mV peak-to-peak using ac signals at OCP. The inhibition efficiencies (IE%) and the surface coverage (θ) obtained from the impedance measurements are defined by the following Eq. 9:

$$\text{IE\%} = \theta \times 100 = [1 - (R_{ct}/R_{ct(inh)})] \times 100 \tag{9}$$

where R_{ct} and $R_{ct(inh)}$ are the charge transfer resistances in the absence and presence of inhibitor, respectively.

The main parameters deduced from the analysis of Nyquist diagram are the resistance of charge transfer R_{ct} (diameter of high frequency loop) and the capacitance of double layer C_{dl} which is defined as Eq. 10:

$$C_{dl} = (2\Pi R_{ct}F_{max})^{-1} \tag{10}$$

where F_{max} is the maximum frequency at which the imaginary component (Zimag) of the impedance is maximum; since the electrochemical theory assumed that $1/R_{ct}$ is directly proportional to the capacity of double layer.

3 Results and discussion

3.1 FTIR spectroscopy of *P. oceanica*/PVP

The FTIR of *P. oceanica*/PVP extracts in Figure 1 shows that the broad IR peak is located at 3,332 cm^{-1} and this may be attributed to the ν_{st} of the O–H and N–H groups interested in the compounds of phenolic and proteins, respectively. In addition, the ν_{ast} and ν_{st} of C–O–C polysaccharide glycosidic linkage are located at 1,250 and 1,044 cm^{-1}, respectively [19,20]. The two sharp IR peaks are centered at 2,915 and 2,849 cm^{-1} corresponding to the ν_{ast} and ν_{st} of CH_2 in fatty acids, respectively [21]. This indicates that the ethanolic extracts of *Posidonia oceanica* are lipid-rich materials. Furthermore, the FTIR peaks arising from the existence of C═O located at 1,727 and 1,634 cm^{-1} are corresponding to the ester and carboxylic group of lipids and PVP, respectively. The FTIR peak located at 1,170 cm^{-1} is attributed to the (C–O) group. This IR peak confirmed the existence of fatty acids long-chain (C_{22}–C_{34}), such as palmitic molecules, linoleic, palmitoleic, and oleic acids [22].

Figure 1 shows that the "fingerprint" region (i.e., 900–400 cm^{-1}) was detected for the polysaccharide molecules, such as the intense FTIR peak located at 867 cm^{-1} which is considered to conform to the mannose and galactose pyranose rings [23]. Additionally, the peaks located at ~718 and 648 cm^{-1} are assigned to the existence of xylans-type polysaccharides [24]. These peaks support the presence of carbohydrate compounds [25]. The two weak FTIR peaks centered at 3,740 and 3,696 cm^{-1} are attributed to the inner OH of kaolin [26,27]. The FTIR confirmed the existence of phenolic and polysaccharide compounds with traces of kaolin.

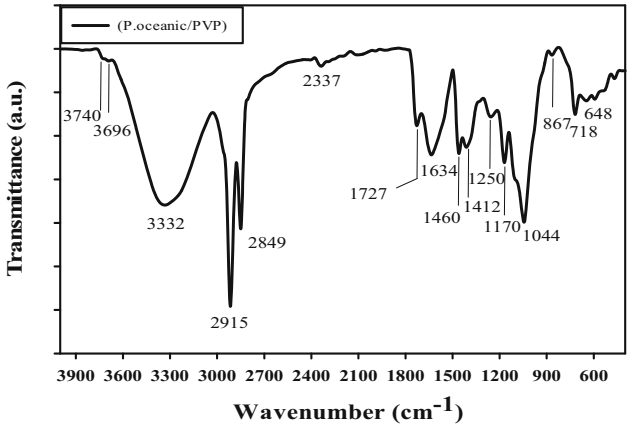

Figure 1: FTIR of ethanolic *Posidonia oceanica* based on PVP extracts.

3.2 Gravimetric estimation (weight loss approach)

To examine the impact of the concentrates expansion of ethanolic *Posidonia oceanica* based on PVP, various focuses on the erosion of steel in corrosive media of 1 M of HCl arrangement were tried and concentrated by weight reduction estimations at 20°C after a period of 120 h. Figure 2 outlines the weight reduction time bent for the erosion of mild steel in corrosive media in the absence and existence of the numerous contents of ethanolic extracts inhibitor of *P. oceanica*/PVP at 20°C. The current results indicated that the weight losses of steel samples in the existence of *P. oceanica*/PVP were lower than that of free (blank) samples in the corrosive media. It expanded and shifted directly over time for all focuses. The acquired linearity demonstrated the lack of insoluble surface film through erosion. First, the *P. oceanica*/PVP inhibitor was immobilized onto the metal sample surface, blocking the corrosion process in this way [28]. These observations led to the conclusion that the ethanolic

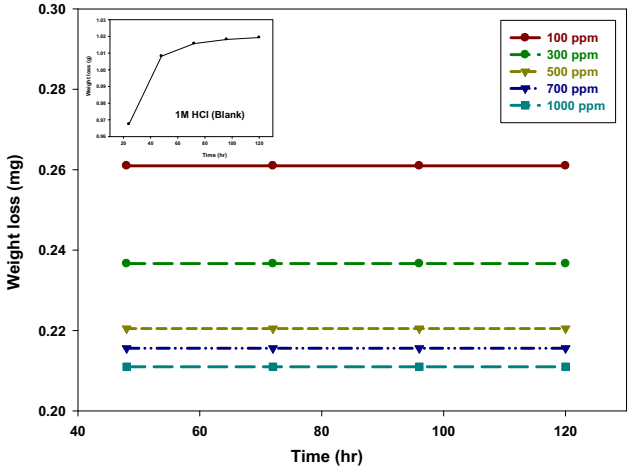

Figure 2: Weight loss-time dependence curve for the corrosion of steel in corrosive media of 1 M of HCl in the presence and absence of various concentrations of ethanolic extracts of *P. oceanica*/PVP at a temperature of 20°C.

Table 1: Corrosion parameters such as CR, θ, and IE% of mild steel in corrosive media (1 M of HCl) in the presence and absence of various concentrations of ethanolic extract of *P. oceanica*/PVP obtained by weight-loss approach at a temperature of 20°C

Inhibitor concentration (ppm)	Corrosion rate (CR) (mm/year)	Surface coverage (θ)	Inhibition efficiency (IE) (%)
Blank	210.440	—	—
100	55.456	0.741	74
300	52.000	0.754	75
500	50.230	0.759	76
700	46.240	0.782	78
1,000	45.376	0.787	79

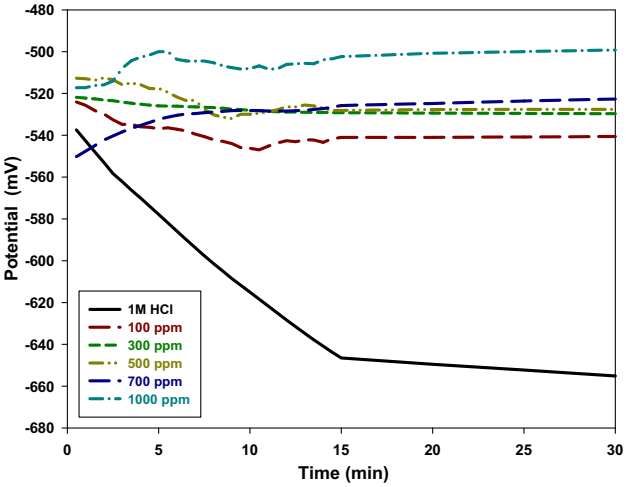

Figure 3: Corrosion potential–time dependence curve for the corrosion of mild steel in corrosives media (1 M of HCl) in the absence and presence of the various concentrations of *P. oceanica*/PVP at a temperature of 20°C.

extracts of *P. oceanica*/PVP are selected as a steel disintegration inhibitor in the corrosive solution. Table 1 outlines the corresponding inhibition effectiveness, the coverage of the surface, and the erosion rate percentage data measured using the 120 h weight reduction results. This tends to be observed from the fact that the expansion of extracts reduces the erosion rate and indicates obvious consumption restraint conducted against the erosion of steel in corrosive media. The inhibitory impact is incrementing through expanding the convergence of ethanolic extracts of *P. oceanica* based on PVP. The maximum IE% of 79% was obtained at 1,000 ppm for this inhibitor. The change in the value of IE% with the concentrations (Table 1) revealed that the ethanolic extracts were concentration-dependent inhibitors. It was postulated that the exceptionally low corrosion rates with the use of an inhibitor which is relative to the free solution were due to the influence on the metal surface of a thin and stable passive layer [29]. In groups C–O, O–H, and C═O and other aromatic molecules, the concentrates contain oxygen atoms which are rich in electrons and can fill in the metal surface along these lines as a good adsorption site that restricts the mild steel corrosion in corrosive media.

3.3 OCP estimations

The steel electrochemical activity in corrosive media was evaluated over time by measuring the alternation of the corrosion potential (E_{corr}). Changes in OCP in the existence and absence of *P. oceanica*/PVP inhibitor in corrosive media of 1 M of HCl are presented in Figure 3. The potential accomplishes a consistent state at 30 min after the introduction. It has been observed that the OCP rapidly changes toward negative qualities without the inhibitor of *P. oceanica*/PVP. This displays the pre-immersion, the disintegration mechanism of air-framed oxide layer, and the attack on the surface of the metal. Compared with the free sample, a steady potential was easily achieved. For various concentrations, the steady-state potential of mild steel in corrosives media shifted further toward a positive value. This is due to the inhibitor adsorption of *P. oceanica*/PVP on the surface of the metal sample and this results in metal passivation [30]. Physical adsorption takes place among the positive (+ve) charge of the protonated *P. oceanica*/PVP inhibitor and the negative (–ve) charge of the steel surface ($FeCl_3$) in corrosive media of HCl. As a result, E_{corr} drifts to more +ve values in the steady-state. In any case, it is shown from Figure 3 that the positive move of E_{corr} is too little for a sensible arrangement dependent on the results of the OCP estimations.

3.4 PP estimation

Figure 4 shows the PP curves of steel samples in the corrosive media in the absence and existence of various *Posidonia oceanica* ethanolic extracts dependent on the PVP inhibitor concentrations. Numerous corrosion parameters, such as corrosion potential (E_{corr}), anodic and cathodic Tafel slopes (β_a and β_c), corrosion current density (I_{corr}), polarization resistance (R_p), and inhibition efficiency (IE%), are shown in Table 2. It can be very well shown that the inhibitor extract of *P. oceanica*/PVP has a small impact on the anodic Tafel consistent estimates and a more important impact on the cathodic Tafel steady estimates. This demonstrates that the inhibitor

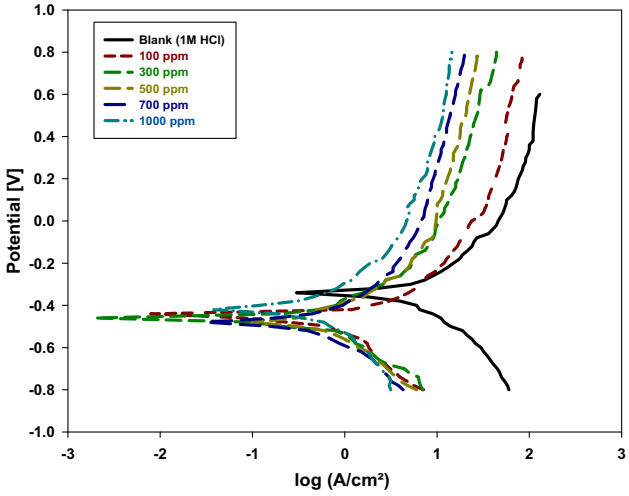

Figure 4: PP curve for mild steel in corrosive media of 1 M of HCl solutions in the absence and existence of the different concentrations of *P. oceanica*/PVP at a temperature of 20°C.

can alert the instrument of cathodic response and may not have an effect on the anodic disintegration phase [31]. Figure 4 shows that the hydrogen advancement is activation-controlled. In addition, it demonstrates that the decrease instrument of anodic is not influenced by the existence of the *P. oceanica*/PVP inhibitor. The change in the values of the cathodic Tafel slope (β_c) is proposing that the response component of hydrogen decrease is not equivalent to the existence and absence of *P. oceanica*/PVP. The information in Table 2 clearly shows that the current density (I_{corr}) values decrease, and the polarization values (R_p) increase as predicted by the existence of different percentages of *P. oceanica*/PVP. The values of mild steel I_{corr} in the inhibited solution are more modest than those of the free solution of the inhibitor. Due to the reverse relationship between R_p and I_{corr} through expanding the concentration of the *P. oceanica*/PVP inhibitor, it is commonly assumed that the adsorption of the *P. oceanica*/PVP inhibitor particles takes place on the metal surfaces by creating physical and charge-transfer barriers to protect the metal surfaces in a high degree. The inhibiting activity expanded by the concentration is at the highest estimation of 81% at 1 g/L (1,000 ppm). The E_{corr} value moved toward the negative direction by incorporating the ethanolic extracts of *Posidonia oceanica*. In addition, the change in the negative corrosion potential suggests that the compounds examined by *P. oceanica*/PVP are considered cathodic inhibitor [32]. The abatement of the erosion current density and the expansion of the hindrance effectiveness might be credited to the physical adsorption of the investigated compounds of the *P. oceanica*/PVP inhibitors on the metal surface sample. The results of the tests based on polarization curves revealed that I_{corr} decreases dramatically in the presence of the *P. oceanica*/PVP inhibitor at all studied concentrations. The Tafel polarization technique affirmed the results of the main weight reduction, giving some extra data. They are dictated by the extrapolation of Tafel lines to the corrosion potentials. Table 3 shows the examination of hindrance productivity estimated by weight reduction technique and PP. Additionally, it is observed from Table 3 that polarization studies have a close relationship with the estimations of inhibition efficiencies which were obtained by using the *P. oceanica*/PVP inhibitors through weight reduction estimations.

Table 3: Comparison of inhibition efficiency of *P. oceanica*/PVP measured by weight reduction method and PP

Inhibitor concentration (ppm)	Inhibition efficiency (%)	
	Weight loss method	PP
100	74	55
300	75	68
500	76	75
700	78	80
1,000	79	81

Table 2: The parameters of the corrosion experiment obtained from polarization curves for mild steel in 1 M of HCl solution in the absence and existence of the various *P. oceanica*/PVP concentrations at a temperature of 20°C

Inhibitor concentration (ppm)	E_{corr} (V)	I_{corr} (μA/cm^2)	β_a (V/dec)	β_c (V/dec)	R_p (Ω·cm^{-2})	CR (μm/year)	θ	IE (%)
1 M of HCl (blank)	−0.345	7.925	1.20	0.66	21916.27	61.629	—	—
100	−0.428	3.548	0.40	0.10	24475.0	27.592	0.5523	55
300	−0.463	2.512	1.20	0.30	41487.5	19.534	0.6830	68
500	−0.481	1.995	1.86	0.34	63031.7	15.516	0.7482	75
700	−0.475	1.585	1.20	0.30	65753.0	12.325	0.8000	80
1,000	−0.416	1.514	1.33	0.40	88266.9	11.770	0.8090	81

3.5 EIS

EIS is a non-destructive method that provides information about surface properties. The Nyquist and Bode plots of mild steel in 1 M of HCl with and without the various concentrations of *P. oceanica*/PVP at OCP are shown in Figure 5. The Nyquist plot in Figure 5a is a semicircle which shows that its diameter increases with the increase in the *P. oceanica*/PVP concentration. The high half-circle is credited to the double-layer capacitance [33]. It is obvious that the impedance spectra are not an ideal half-circle and are a discouraged capacitive circle compared with the surface heterogeneity which might be the consequence of the surface unpleasantness or adsorption of the inhibitor atoms [33–35]. The charge transfer resistance value increases with the increase in the *P. oceanica*/PVP concentration. Its value is a measure of electron transfer across the surface and is inversely proportional to the corrosion rate [36]. Figure 5b and c shows that the Bode plot shapes for the inhibited and uninhibited mild steel does not change. This indicates that the *P. oceanica*/PVP inhibitor does not change the corrosion mechanism. Figure 5d demonstrates the proposed inhibitor corrosion mechanism of *P. oceanica*/PVP. The EIS parameters are listed in Table 4. From R_{ct}, the IE% increases with the increase in the *P. oceanica*/PVP concentration. The results obtained from EIS are consistent with the results observed by the polarization and weight-loss measurements. This indicates the ability of *P. oceanica*/PVP as a corrosion inhibitor for mild steel in 1 M of HCl solution.

3.6 Adsorption isotherm

The inhibitor compounds' adsorption depends on several factors: the charge on the surface of the metal and their composition, the electronic characteristics of the metal surface when the other ionic species and solvents are adsorbed, the electrochemical potential, and the corrosion reaction temperature at the interface of the metal solution [37]. As a result, the division of surface covered with inhibitor species (θ) will occur as a part of inhibitor fixation and solution temperature. The information on surface inclusion (θ) is extremely valuable in discussing the adsorption attributes. Adsorption isotherm could be assessed at harmony condition at the point when the covered part of the surface is resolved as a component of the fixation at a consistent temperature. The level of surface inclusion θ for various *P. oceanica*/PVP concentrations in acidic corrosive media has been assessed by weight reduction and potentiodynamic estimations. The adsorption isotherms and connected mechanisms were drawn. Several mathematical formulae of adsorption isotherms have been proposed to match the experimental data in this study, but the best fit was found through the equation of Langmuir adsorption isotherm, which is as follows [35]:

$$C/\theta = 1/K_{ads} + C \tag{11}$$

where K_{ads} and C are the equilibrium constants of both the desorption and adsorption process and the various concentrations of *P. oceanica*/PVP, respectively. K_{ads} values can be calculated by the intercepts of the straight line of the C/θ axis which is related to the standard free energy of adsorption (ΔG^0_{ads}), as calculated in the following Eqs. 12 and 13:

$$K_{ads} = 1/55.5 \exp^{(-(\Delta G_{ads}/RT))} \tag{12}$$

or

$$\Delta G^0_{ads} = -RT \ \ln(55.5K_{ads}) \tag{13}$$

where R and T are the gas constant and the absolute temperature, respectively. The water concentration in the bulk solution has a value of 55.5. The values of free energy, ΔG^0_{ads}, were calculated.

Table 4 displays the calculated free energy values (ΔG^0_{ads}) of mild steel samples in corrosive media of 1 M of HCl in the existence and absence of the various concentrations of *P. oceanica*/PVP. The –ve values of free energy (ΔG^0_{ads}) indicate the continuous adsorption of the *P. oceanica*/PVP inhibitors on the surface of steel samples [35]. Generally, the estimations of free energy (ΔG^0_{ads}) up to $-20\ kJ{\cdot}mol^{-1}$ are steady with electrostatic interactions (physical adsorption) among charged metal and atoms, while the estimations of free energy (ΔG^0_{ads}) around or higher than $-40\ kJ{\cdot}mol^{-1}$ are related to a direct chemisorption result by moving or sharing electrons from the *P. oceanica*/PVP inhibitor particles to the metal surface to frame coordinate bonds. The adsorption modes, such as physisorption adsorption modes and chemisorption adsorption modes, could be ascribed to the fact that the investigated *P. oceanica*/PVP inhibitors contain several chemical compounds that may be adsorbed physically or chemically [38]. The plot of the C/θ virus contraction of the *P. oceanica*/PVP inhibitors for mild steel in corrosive media with and without the various concentrations of *P. oceanica*/PVP is a linear relationship, as shown in

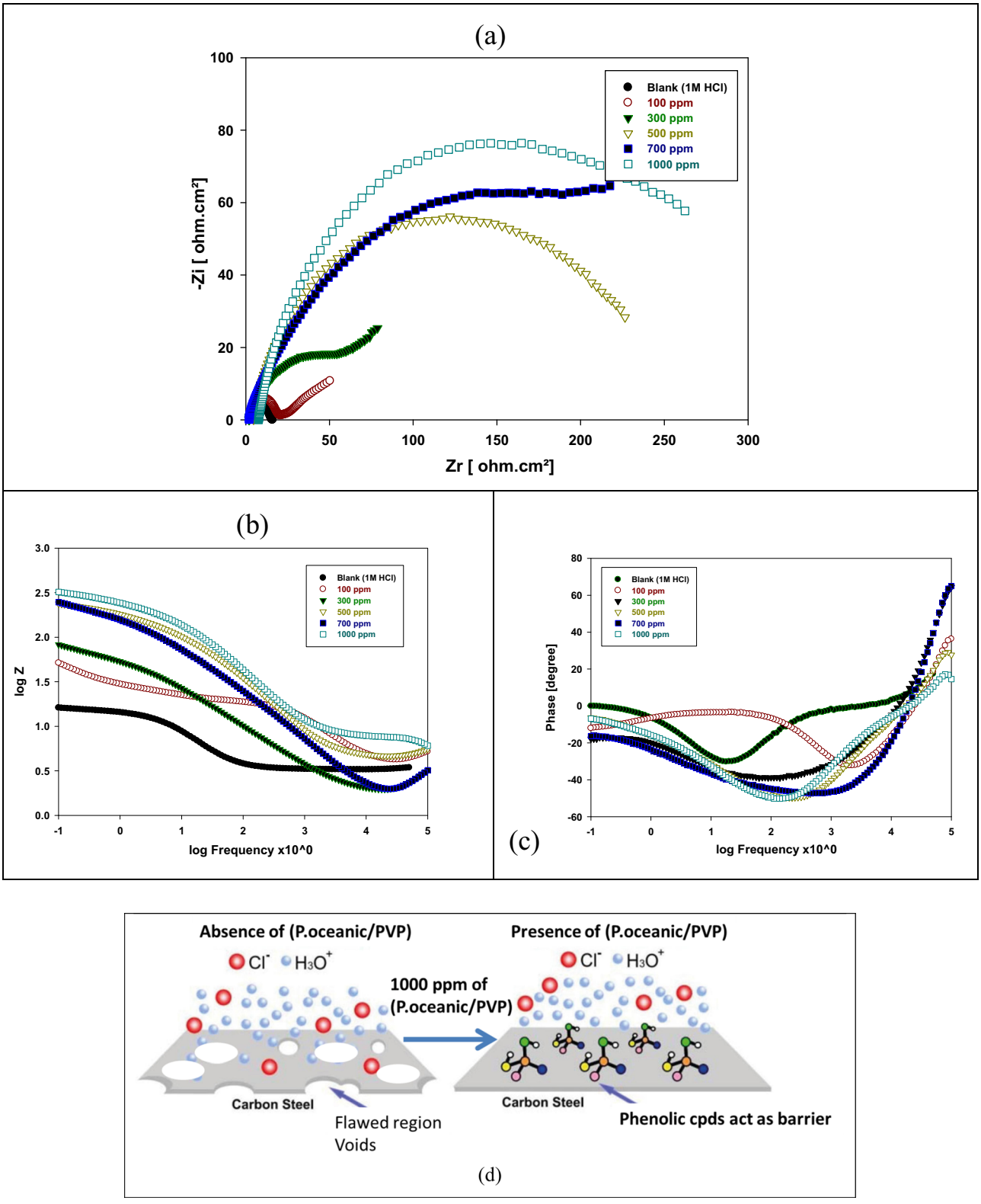

Figure 5: EIS plots as (a) Nyquist plot, (b) Bode plot, (c) phase angle plot for mild steel in 1 M of HCl with and without the various concentrations of *P. oceanica*/PVP and (d) proposed mechanism of *P. oceanica*/PVP as corrosion inhibitor.

Table 4: EIS parameters for mild steel in 1 M of HCl with and without the various concentrations of *P. oceanica*/PVP

Inhibitor concentration (ppm)	R_s (Ω·cm^2)	R_{ct} (Ω·cm^2)	C_{dl} (μF·cm^2)	Phase angle	IE (%)
1 M of HCl (blank)	3.25	12.13	183.1	−10.4	—
100	1.210	16.51	152.3	−26.2	26.5
300	1.958	102.1	21.27	−20.4	88.1
500	2.460	241.8	17.83	−18.5	94.9
700	3.354	319.1	8.633	−20.8	96.2
1,000	4.250	333.6	1.331	−18	96.4

Figure 6. This indicates that the physical adsorption approach of *P. oceanica*/PVP to the metal surface sample is following Langmuir adsorption isotherm (Table 5).

3.7 The effect of temperature on inhibition process

To detect the stability of the formed protective film, the corrosion rate of the investigated inhibitor was studied at different temperatures (20°C, 40°C, and 50°C) for 3 h. The effect of temperature on the corrosion rate of mild steel in 1 M of HCl solutions in the absence and presence of the best *P. oceanica*/PVP concentration (1,000 ppm) was obtained by the weight-loss method. The effect of temperatures on the inhibited steel surface is highly complex because many changes occur on the metal surface. As the temperature increases, the degree of the surface coverage decreases due to the inhibitors' desorption from the steel surface. The surface becomes less protected and the inhibition, therefore, gradually looses its effectiveness.

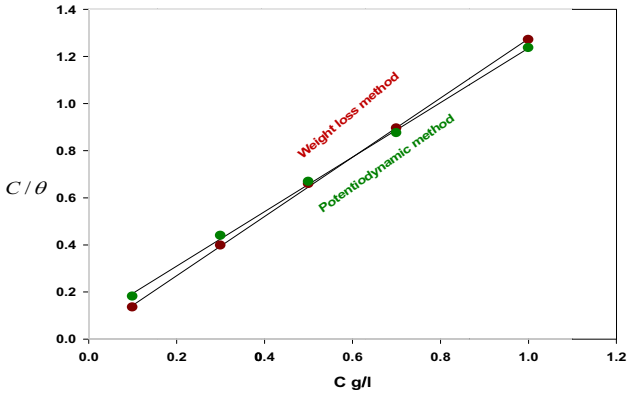

Figure 6: Langmuir adsorption isotherm model for mild steel in corrosive media (1 M of HCl) in the existence and absence of *P. oceanica*/PVP at a temperature of 20°C through weight loss and potentiodynamic approach.

The apparent activation energy value (E_a) was calculated using the Arrhenius equation as given in Eq. 14:

$$\text{C.R.} = A \exp - E_a/RT \tag{14}$$

where C.R. is the corrosion rate of the mild steel surface, A is the Arrhenius constant or the pre-exponential factor, R is the universal gas constant, and T is the absolute temperature.

Figure 7 shows that the linear regression plots between ln C.R. and $1/T$ give a slope of $-E_a/R$. The calculated activation energy (E_a) and regulation factor (R) for mild steel in 1 M of HCl solutions in the absence and presence of *P. oceanica*/PVP are displayed in Table 6. The values of E_a may be explained by the modification of the corrosion process mechanism in the presence of inhibitor molecules. The activation energy of the inhibited metal is higher than the uninhibited one. This indicates that more energy barriers are required for the corrosion reaction. According to several reports, the activation energy E_a due to chemical adsorption (>80 kJ·mol^{-1}) is considerably larger than that due to physical adsorption (<80 kJ·mol^{-1}).

The values of apparent enthalpy of activation ΔH_{ads} and entropy of activation ΔS_{ads} were obtained by the linearized transition state theory. As shown in Figure 8,

Table 5: Parameters of Langmuir adsorption isotherm in corrosive media of 1 M of HCl for mild steel in the presence and absence of *P. oceanica*/PVP at a temperature of 20°C through weight loss and potentiodynamic approach

Investigated inhibitor	Weight reduction method				Potentiodynamic method			
	Slope	K_{ads}	R^2	ΔG_{ads}	Slope	K_{ads}	R^2	ΔG_{ads}
P. oceanica/PVP	1.2575	56.863	0.9996	−19.627	1.1573	12.802	0.9989	−15.995

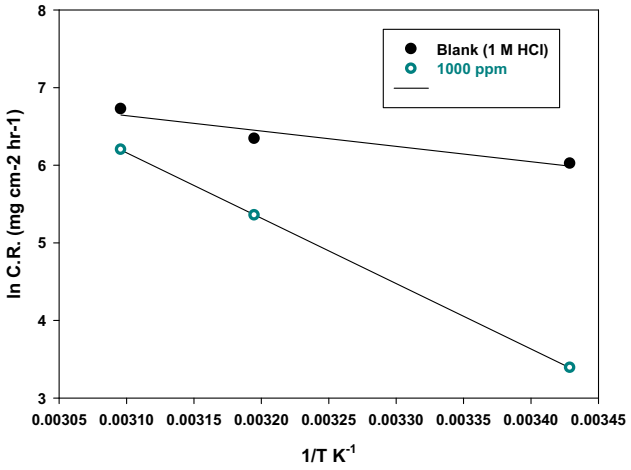

Figure 7: A plot of ln C.R. versus 1/*T* for mild steel in 1 M of HCl solutions in the absence and presence of the best *P. oceanica*/PVP concentration (1,000 ppm).

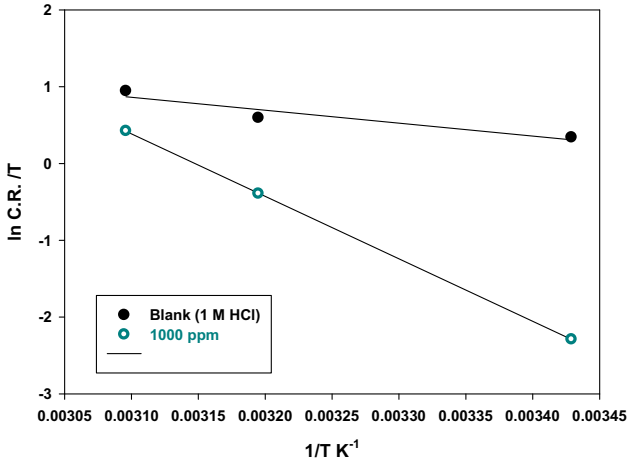

Figure 8: A plot of ln C.R./*T* versus 1/*T* for mild steel in 1 M of HCl solutions in the absence and presence of the best *P. oceanica*/PVP concentration (1,000 ppm).

the values of ΔH_{ads} and ΔS_{ads} listed in Table 6 were calculated using the slope and the intercept of the straight line of ln CR/*T* versus 1/*T*, respectively. The positive values of ΔH show that the *P. oceanica*/PVP adsorption on the steel surface is endothermic. This means that the dissolution of steel is difficult. However, the negative values of ΔS_{ads} in the presence of the inhibitor imply that the activated complex in the rate-determining step is an association rather than a dissociation step. The increase in entropy in the presence of *P. oceanica*/PVP indicates that the increase in the disorder takes place in going from reactants to the film formed on the metal/solution interface.

3.8 Mechanism inhibition process

The physical adsorption of *P. oceanica*/PVP molecules on the surface of the metal steel sample increased with the increase in the *P. oceanica*/PVP concentration. It was suggested that the high lipid content of *P. oceanica*/PVP (Figure 1) arises from the existence of C=O at 1,727 and 1,634 cm^{-1} and the additional peaks correspond to carbonyl moiety in lipids molecules. The C–O groups also show an IR peak at 1,170 cm^{-1}. These IR peaks confirmed the existence of long-chain (C_{22}–C_{34}) fatty acids, such as palmitoleic, palmitic, linoleic, and oleic acids, which correspond to the general concept of traditional corrosion inhibitors. The non-fortified oxygen electrons are protonated in acidic media. Due to the electrostatic interactions, the protonated *P. oceanica*/PVP particles are adsorbed physically. The erosion hindrance happens because of the adsorption of natural atoms at the interface of metal/solution. The adsorption process itself relies on the particle's composition, temperature, and the electrochemical potential at the interface of metal/solution. The H_2O molecules are adsorbed on the metal surface to form the interface of metal/solution. In addition, some adsorbed molecules of H_2O may occur on the metal surface by the *P. oceanica*/PVP inhibitor.

The mechanism of steel sample corrosion in corrosive media of 1 M of HCl is shown in Eq. 15:

$$Fe \rightarrow Fe^{2+} + 2e^{-} \quad (15)$$

There are different cathodic reactions that are the most common reactions in acidic media [10]:

$$2H^{+} + 2e^{-} \rightarrow H_2 \quad (16)$$

$$O_2 + 4H^{+} + 4e^{-} \rightarrow 2H_2O \quad (17)$$

Table 6: Thermodynamic parameters obtained by weight-loss method

Parameters	R^2	E_a (kJ/mol)	ΔH_{ads} (kJ/mol)	ΔS_{ads} (kJ/mol)
Blank (1 M of HCl)	0.9238	16.412	13.994	–146.960
1,000 ppm	0.9999	70.015	67.617	–26.182

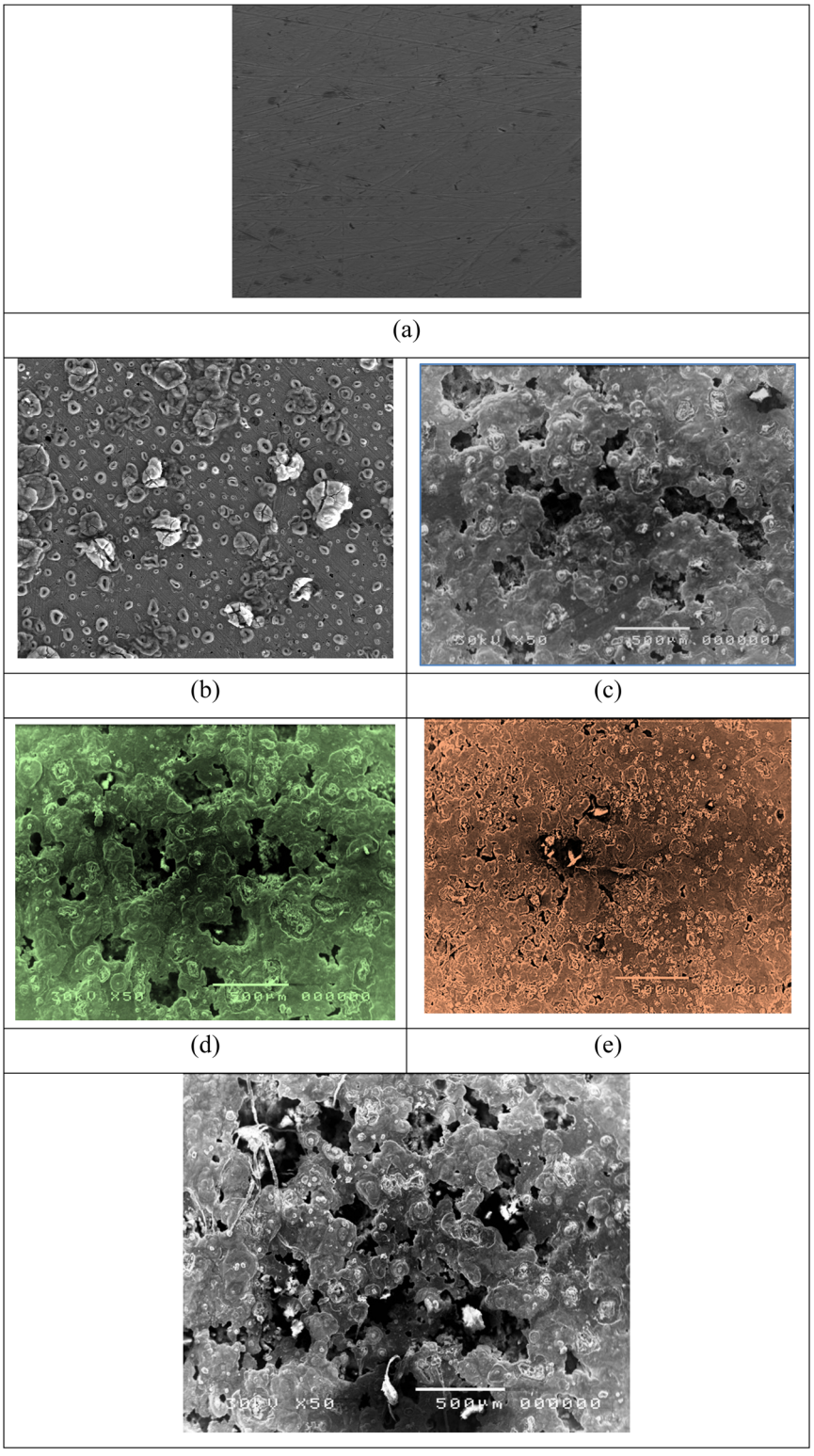

Figure 9: SEM micrographs of blank polished steel samples (a), after an immersion in corrosive media of 1 M of HCl in the absence of *P. oceanica*/PVP (b), after a soak in corrosive media of 1 M of HCl in the existence of 100 ppm of *P. oceanica*/PVP (c), after a soak in corrosive media of 1 M of HCl in the existence of 300 ppm of *P. oceanica*/PVP (d), after a soak in corrosive media of 1 M of HCl in the existence of 1,000 ppm of *P. oceanica*/PVP (e), and after a soak in corrosive media of 1 M of HCl in the existence of 1,000 ppm of PVP (f).

When iron corrodes, the rate is usually controlled by the cathodic reaction.

$$Fe + HCl \rightarrow FeCl_2 + H_2 \quad (18)$$

Fe is oxidized to Fe^{2+} by H^+; the Cl^- ion was not strong enough to act as an oxidizing agent so it plays no role in the reaction according to Le Chatelier's principle. In the reduction reaction, the hydrogen gas evolution is as follows:

$$2H^+ + 2e^- \rightarrow H_{ads} + 2H_2 \quad (19)$$

where H_{ads} is the adsorbed hydrogen ions on the surface of the steel sample which acts as a catalyst to enhance the generation of the new bubble of hydrogen gas in the surface of the cathode [39–41]. The percent of *P. oceanica*/PVP can prevent hydrogen gas generation and stop the corrosion process.

3.9 Spectroscopic analysis of mild steel

Figure 9 represents the SEM micrographs of the steel samples in the corrosive media of 1 M of HCl after 120 h in the existence and absence of *P. oceanica*/PVP. In addition, this figure collects the macrostructure of the polished samples before cathodic corrosion, the corroded samples of blank samples, and at the concentrations of 100, 300, and 1,000 ppm in the investigated inhibitors. The scanning electron micrographs show the protective film formed on the surface of the steel sample by *P. oceanica*/PVP. Figure 9b shows that the specimen surface of the mild steel is extensively oxidized and rougher. Additionally, it strongly damaged the blank sample. On the other hand, Figure 6c–e shows that forming a protective layer on the surfaces of the steel samples results in a safer and clearer surface for the examined inhibitors. This protective sheet of *P. oceanica*/PVP could act as an isolate and barrier to the vulnerable surface of the steel in corrosive environments. The extent of damage on the surface of the steel sample and the rate of steel sample corrosion is considerably lower in the existence of inhibitors, especially at high concentration of 1,000 ppm. This revealed that there was a good defensive film adsorbed on the metal surface that acted as a physical and charged barrier and which was responsible for the inhibition of erosion. The SEM micrographs show an adherence of the inhibitors on the metallic surfaces which are in acceptable concurrence with the results of the electrochemical estimation. While the metallic surfaces were coated with 1,000 ppm of PVP, they were strongly damaged. They also showed big voids on the steel surface (Figure 9f).

4 Conclusion

The accompanying ends might be drawn from the examination: ethanolic extract concentrates of *P. oceanica*/PVP in the hydrochloric corrosion have been discovered to be a solid inhibitor of mild steel erosion. The restraint effectiveness increments with an inhibitor focused on achieving an estimation of 81% at 1,000 ppm. Polarization measurements show that the ethanolic extracts of *P. oceanica*/PVP act as a cathodic inhibitor. The model of adsorption mechanism of *P. oceanica*/PVP on steel surface fitted the equation of Langmuir adsorption isotherm and was physisorption. The inhibitor efficiency determined by the electrochemical polarization and the gravimetric method is in good agreement.

Funding information: Authors state no funding involved.

Author contributions: Ghalia A. Gaber: writing – original draft, methodology, formal analysis; Mohamed Mohamady Ghobashy: writing – original draft, formal analysis, visualization; Mohamed Madani: methodology, writing – review and editing; Dalal Mohamed Alshangiti: methodology, formal analysis, writing; Sheikha A. Alkhursani: methodology, formal analysis, writing; Samera Ali Al-Gahtany: methodology, formal analysis, writing – review and editing; Norhan Nady: methodology, formal analysis, resources, supervision, writing – review and editing. All authors have read and agreed to the published version of the manuscript.

Conflict of interest: Authors state no conflict of interest.

Data availability statement: All data generated or analyzed during this study are included in this published article.

References

[1] Benito-González I, López-Rubio A, Martínez-Abad A, Ballester A-R, Falcó I, González-Candelas L, et al. In-depth characterization of bioactive extracts from Posidonia oceanica waste biomass. Mar Drugs. 2019;17:409. doi: 10.3390/md17070409.

[2] Karungamye PN, Murthy HA. Methanolic extract of Adansonia digitata (Baobab) fruit pulp and seeds as potential green inhibitors for mild steel corrosion in 0.5 MH $2SO_4$ solutiom. Ind J Adv Chem Sci. 2017;5:295–305. doi: 10.9790/5736-1007016474.

[3] Kaur K, Jain P, Sobti A, Toor AP. Sulfated metal oxides: eco-friendly green catalysts for esterification of nonanoic acid with

methanol. Green Process Synth. 2016;5:93–100. doi: 10.1515/gps-2015-0087.
[4] Bubalo MC, Sabotin I, Radoš I, Valentinčič J, Bosiljkov T, Brnčić M, et al. A comparative study of ultrasound-, microwave-, and microreactor-assisted imidazolium-based ionic liquid synthesis. Green Process Synth. 2013;2:579–90. doi: 10.1515/gps-2013-0086.
[5] Shehata OS, Korshed LA, Attia A. Green corrosion inhibitors, past, present, and future. Corrosion inhibitors, principles and recent applications. Croatia: InTech Publishing Inc; 2018. p. 121–42. doi: 10.5772/intechopen.72753.
[6] Gupta P, Jain G. Corrosion inhibition by Aloe barbadensis (aloe vera) extract as green inhibitor for mild steel in HNO3. IJSRR. 2014;3:72–83.
[7] Singh A, Kumar A, Pramanik T. A theoretical approach to the study of some plant extracts as green corrosion inhibitor for mild steel in HCl solution. Orient J Chem. 2013;29:277–83.
[8] Sanaei Z, Shahrabi T, Ramezanzadeh B. Synthesis and characterization of an effective green corrosion inhibitive hybrid pigment based on zinc acetate-Cichorium intybus L leaves extract (ZnA-CIL. L): electrochemical investigations on the synergistic corrosion inhibition of mild steel in aqueous chloride solutions. Dyes Pigm. 2017;139:218–32. doi: 10.1016/j.dyepig.2016.12.002.
[9] Grossmann A, Sora K. Green processing and synthesis. Green Process Synth. 2012;1(5):405–5.
[10] Ghobashy MM, Alshangiti DM, Alkhursani SA, Al-Gahtany SA, Shokr FS, Madani M. Improvement of in vitro dissolution of the poor water-soluble amlodipine drug by solid dispersion with irradiated polyvinylpyrrolidone. ACS omega. 2020;5:21476–87. doi: 10.1021/acsomega.0c01910.
[11] Ghobashy MM, Elhady MA. pH-sensitive wax emulsion copolymerization with acrylamide hydrogel using gamma irradiation for dye removal. Radiat Phys Chem. 2017;134:47–55. doi: 10.1016/j.radphyschem.2017.01.021.
[12] Ghobashy MM. Combined ultrasonic and gamma-irradiation to prepare TiO2@PET-g-PAAc fabric composite for self-cleaning application. Ultrason Sonochem. 2017;37:529–35. doi: 10.1016/j.ultsonch.2017.02.014.
[13] Ghobashy MM, El-Damhougy BK, El-Wahab HA, Madani M, Amin MA, Naser AEM, et al. Controlling radiation degradation of a CMC solution to optimize the swelling of acrylic acid hydrogel as water and fertilizer carriers. Polym Adv Technol. 2021;32:514–24. doi: 10.1002/pat.5105.
[14] Horváth R, Lindvold LR, Larsen NB. Fabrication of all-polymer freestanding waveguides. J Micromech Microeng. 2003;13:419. doi: 10.1088/0960-1317/13/3/310.
[15] Wang F, Wang X. Mechanisms in the solution growth of free-standing two-dimensional inorganic nanomaterials. Nanoscale. 2014;6:6398–414. doi: 10.1039/C4NR00973H.
[16] Khandelwal R, Arora S, Mathur S. Study of plant Cordia dichotoma as green corrosion inhibitor for mild steel in different acid media. EJ Chem. 2011;8:1200–5. doi: 10.1155/2011/164589.
[17] Ghanem WA, Ghayad I, Gaber G. Corrosion behavior of reinforcing steel in cement partially replaced with metakaolin in 3.5% NaCl and 5% $MgSO_4$ solution. Inter J Metall Mater Sci Eng. 2013;3:1–8.
[18] Tu W, Cheng Y, Zhan T, Han J, Cheng Y. Influence of sodium tungstate and sealing treatment on corrosion resistance of coatings formed on AZ31 magnesium alloy by plasma electrolytic oxidation. Int J Electrochem Sci. 2017;12:10863–81. doi: 10.20964/2017.11.34.
[19] Sayari N, Balti R, Mansour MB, Amor IB, Graiet I, Gargouri J, et al. Anticoagulant properties and cytotoxic effect against HCT116 human colon cell line of sulfated glycosaminoglycans isolated from the Norway lobster (Nephrops norvegicus) shell. Biomed Pharmacother. 2016;80:322–30. doi: 10.1016/j.biopha.2016.03.027.
[20] Xu Y, Cai F, Yu Z, Zhang L, Li X, Yang Y, et al. Optimisation of pressurised water extraction of polysaccharides from blackcurrant and its antioxidant activity. Food Chem. 2016;194:650–8. doi: 10.1016/j.foodchem.2015.08.061.
[21] Forfang K, Zimmermann B, Kosa G, Kohler A, Shapaval V. FTIR spectroscopy for evaluation and monitoring of lipid extraction efficiency for oleaginous fungi. PloS one. 2017;12:1–17. doi: 10.1371/journal.pone.0170611.
[22] Cornara L, Pastorino G, Borghesi B, Salis A, Clericuzio M, Marchetti C, et al. Posidonia oceanica (L.) delile ethanolic extract modulates cell activities with skin health applications. Mar Drugs. 2018;16:21. doi: 10.3390/md16010021.
[23] Yang X, Huang M, Qin C, Lv B, Mao Q, Liu Z. Structural characterization and evaluation of the antioxidant activities of polysaccharides extracted from Qingzhuan brick tea. Int J Biol Macromol. 2017;101:768–75. doi: 10.1016/j.ijbiomac.2017.03.189.
[24] Schulz H, Baranska M. Identification and quantification of valuable plant substances by IR and Raman spectroscopy. Vib Spectrosc. 2007;43:13–25. doi: 10.1016/j.vibspec.2006.06.001.
[25] Gómez-Ordóñez E, Rupérez P. FTIR-ATR spectroscopy as a tool for polysaccharide identification in edible brown and red seaweeds. Food Hydrocoll. 2011;25:1514–20. doi: 10.1016/j.foodhyd.2011.02.009.
[26] Djomgoue P, Njopwouo D. FT-IR spectroscopy applied for surface clays characterization. J Surf Eng Mater Adv Technol. 2013;3:275–82. doi: 10.4236/jsemat.2013.34037.
[27] Castellano M, Turturro A, Riani P, Montanari T, Finocchio E, Ramis G, et al. Bulk and surface properties of commercial kaolins. Appl Clay Sci. 2010;48:446–54. doi: 10.1016/j.clay.2010.02.002.
[28] Lokesh HB, Sanaulla PF, Bheema VB. An electrochemical investigation on the corrosion behavior of ZA-27 alloy in 1 M Na_2SO_4 in the presence of cationic surfactants as inhibitors. IOSR J Hum Soc Sci. 2001;19:9–20.
[29] Fouda A, Abdel-Maksoud S, Almetwally A. Corrosion inhibition of tin in sodium chloride solutions using propanenitrile derivatives. Chem Sci Trans. 2015;4:161–75. doi: 10.7598/cst2015.970.
[30] Farag AA, El-Din MN. The adsorption and corrosion inhibition of some nonionic surfactants on API X65 steel surface in hydrochloric acid. Corros Sci. 2012;64:174–83. doi: 10.1016/j.corsci.2012.07.016.
[31] Gerengi H, Sahin HI. Schinopsis lorentzii extract as a green corrosion inhibitor for low carbon steel in 1 M HCl solution. Ind Eng Chem Res. 2012;51:780–7. doi: 10.1021/ie201776q.
[32] Ghazi Z, ELmssellem H, Ramdani M, Chetouani A, Rmil R, Aouniti A, et al. Corrosion inhibition by naturally occurring substance containing Opuntia-Ficus Indica extract on the corrosion of steel in hydrochloric acid. J Chem Pharm Res. 2014;6:1417–25.

[33] Ahmed ASI, Ghanem WA, Hussein WA, Gaber GA. Evaluation of some inorganic anions and organic compounds as corrosion inhibitors of Cu–Zn alloys in H_2SO_4 and HNO_3 solutions. Arch Metall Mater. 2020;65:639–51. doi: 10.24425/amm.2020.132803.

[34] Murmu M, Saha SK, Bhaumick P, Murmu NC, Hirani H, Banerjee P. Corrosion inhibition property of azomethine functionalized triazole derivatives in 1 $molL^{-1}$ HCl medium for mild steel: experimental and theoretical exploration. J Mol Liq. 2020;313:113508. doi: 10.1016/j.molliq.2020.113508.

[35] Gaber GA, Maamoun MA, Ghanem WA. Evaluation of the inhibition efficiency of a green inhibitor on corrosion of Cu–Ni alloys in the marine application. Trans Tech Pub. 2018;786:174–94. doi: 0.4028/www.scientific.net/KEM.786.174.

[36] Shahen S, Gaber G. 4-Aminobenzenesulfonic acid as effective corrosion inhibitor for carbon steel in hydrochloric acid. Egypt J Chem. 2021;64:825–34. doi: 10.21608/ejchem.2020.44335.2897.

[37] Deng S, Li X. Inhibition by Ginkgo leaves extract of the corrosion of steel in HCl and H_2SO_4 solutions. Corros Sci. 2012;55:407–15. doi: 10.1016/j.corsci.2011.11.005.

[38] Ating E, Umoren S, Udousoro I, Ebenso E, Udoh A. Leaves extract of Ananas sativum as green corrosion inhibitor for aluminium in hydrochloric acid solutions. Green Chem Lett Rev. 2010;3:61–8. doi: 10.1080/17518250903505253.

[39] Kolb G, Hessel V. Micro-structured reactors for gas phase reactions. Chem Eng J. 2004;98:1–38. doi: 10.1016/j.cej.2003.10.005.

[40] Saeidi S, Najari S, Hessel V, Wilson K, Keil FJ, Concepción P, et al. Recent advances in CO_2 hydrogenation to value-added products –current challenges and future directions. Prog Energy Combust Sci. 2021;85:100905. doi: 10.1016/j.pecs.2021.100905.

[41] Borukhova S, Noël T, Hessel V. Hydrogen chloride gas in solvent-free continuous conversion of alcohols to chlorides in microflow. Org Process Res Dev. 2016;20:568–73. doi: 10.1021/acs.oprd.6b00014.